Development of functionality of metal complexes based on proton-coupled electron transfer

Journal:	*Dalton Transactions*
Manuscript ID	DT-FRO-03-2020-000898.R1
Article Type:	Frontier
Date Submitted by the Author:	11-Apr-2020
Complete List of Authors:	Kojima, Takahiko; University of Tsukuba, Department of Chemistry

Frontiers

Development of functionality of metal complexes based on proton-coupled electron transfer

Takahiko Kojima*[a]

Received 00th January 20xx,
Accepted 00th January 20xx

DOI: 10.1039/x0xx00000x

Proton-coupled electron transfer (PCET) is one of ubiquitous and fundamental processes in various redox reactions performed by transition-metal complexes. In this article, we describe our remarkable achievements related to PCET in metal complexes, including proton manipulation of ligands to afford molecular bistability involving reversible intramolecular PCET and emergence of novel electronic structures, formation and reactivity of Ru^{IV}-oxo and Ru^{III}-oxyl complexes, and mechanistic insights into PCET reactions from O-H and C-H bonds to Ru^{III}-pterin complexes.

Introduction

Proton-coupled electron transfer (PCET) is a ubiquitous and fundamental phenomenon in many kinds of redox reactions. As a basic principle, in a PCET process, a proton is transferred to a proton acceptor and an electron is transferred to an electron acceptor, separately, as described in Scheme 1,[1] in a stepwise or concerted manner. Electron donors are oxidized to reduce electron acceptors and proton donors are deprotonated to

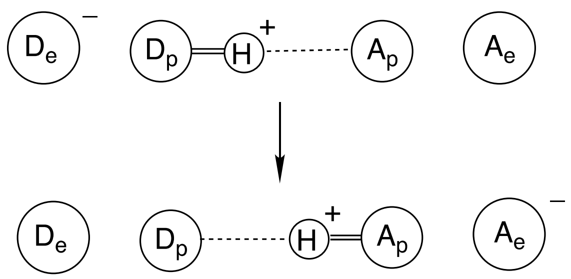

Scheme 1 A schematic description of PCET: D_e, electron donor; D_P, proton donor; A_p, proton acceptor; A_e, electron acceptor.

protonate proton acceptors. PCET can be described as a thermochemical square scheme (Scheme 2) as reported by Mayer and coworkers.[2] The bond dissociation free energy of H-X in PCET is defined as given in eqn 1, where C_{sol} is a solvent-dependent constant, which is essentially $\Delta G°$ ($H^+ + e^- \rightarrow H\bullet$) in a solvent (for CH_3CN, 59.4 kcal mol^{-1} (Fc/Fc^+ as a reference); for H_2O, 55.8 kcal mol^{-1} (NHE as a reference)).[2,3]

$$\mathrm{BDE\ (kcal\ mol^{-1})} = 1.37\,\mathrm{p}K_a + 23.06E_{1/2} + C_{sol} \qquad (1)$$

[a] Department of Chemistry, Faculty of Pure and Applied Sciences, University of Tsukuba, Tsukuba, Ibaraki 305-8571, Japan
[b] E-mail: kojima@chem.tsukuba.ac.jp.

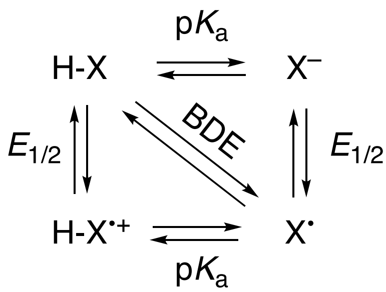

Scheme 2 A thermochemical square scheme for PCET.

Thus, the reactivity of a X-H bond can be argued in light of the bond dissociation energy (BDE) determined by the acidity (pK_a) and the redox potential ($E_{1/2}$).[2b]

In nature, PCET reactions can be found in water oxidation in the Photosystem II (PS II), which is a supramolecular photocatalytic assembly operating in the photosynthesis.[4] In the PS II, a tetranuclear manganese-oxo (Mn-O) cluster, so called "water oxidation complex", acts as a water-oxidation catalyst, which undergoes stepwise photoinduced electron transfer (ET) to afford dioxygen from water *via* the Kok cycle.[5] In the course of the reaction, the Mn-O cluster is converted to be a reactive species *via* PCET oxidation to afford dioxygen.

Inspired by water oxidation in the photosynthesis, Meyer and coworkers have developed an artificial water-oxidation catalyst, which has been known as "the blue dimer".[6] Redox processes in the dimeric μ-oxo Ru(III)-bpy complex have been investigated in the light of a Pourbaix diagram, which is a plot of redox potentials relative to the solution pH values. They have also reported the first example of the formation of a Ru(IV)-oxo complex by PCET oxidation of a Ru(II)-aqua complex using a Ce(IV) salt as an oxidant in water.[7] After the early work by Meyer and coworkers, many examples of formation and reactivity of high-valent Ru-oxo complexes have been reported and deeper insights have been gained into the oxidation reactions by the species.[8,9]

In this article, the author would like to describe our representative achievements in PCET reactions in transition metal complexes. The topics include regulation of redox potentials by proton manipulation to enable intra- and inter-molecular ET reactions, formation and reactivity of Ru(IV)-oxo and electronically equivalent Ru(III)-oxyl complex, PCET reactions of Ru-pterin complexes.

1. Regulation of redox potentials of metal complexes by proton manipulation

Deprotonation and protonation of a ligand bound to a metal centre can control the redox potentials of the metal centre. For example, Haga and coworkers have reported regulation of redox potentials of a tetranuclear $Ru^{II}Os^{II}_3$ complex having benzimidazole moieties in the ligand by deprotonation.[10] The deprotonation of N-H protons of the benzimidazole moieties causes alteration of the order of the redox processes.

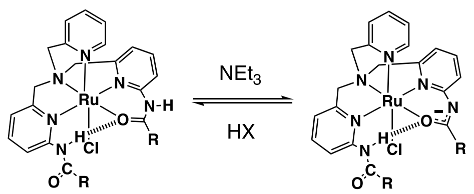

Scheme 3 Reversible deprotonation and protonation of a coordinated amide moiety in a Ru^{II}(bisamide-TPA) complex. R represents functional groups.[11,12]

We have prepared Ru(II) complexes having tris(2-pyridylmethyl)amine (TPA) with functional groups at one or two of the 2-positions of pyridine rings *via* amide linkage.[11] In those complexes, an amide oxygen atom coordinates to the Ru^{II} centre. As for the Ru^{II}(bisamide-TPA) complexes, we have reported that the deprotonation of an amide moiety coordinated to a Ru(II) centre with NEt_3 lowers the redox potential by 500 mV; the original redox potential can be recovered by adding a Brɸnsted acid such as $HClO_4$ (Scheme 3).[12] The deprotonation is enabled by the Lewis acidity of the Ru(II) centre to enhance the acidity of the N-H proton involved in the coordinated amide moiety. Based on this phenomenon, we have synthesized a Ru(II)-Cu(II) dinuclear complex linked by an amide linkage, which is coordinated to the Ru(II) centre through the oxygen atom (Scheme 4).[13] In the starting dinuclear Ru(II)-Cu(II) complex, the redox potential of the Ru^{II}/Ru^{III} redox couple was determined to be +0.69 V (vs. SCE) and that of the Cu^{I}/Cu^{II} couple to be +0.39 V.

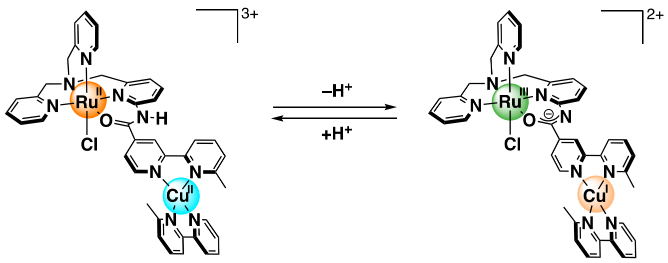

Scheme 4 Proton-coupled electron shuttling between Ru and Cu centres triggered by proton manipulation at the coordinated amide moiety.[13]

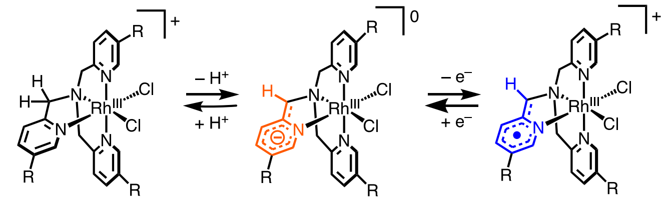

R = H (**1**), $C(O)OCH_3$ (**3**) R = H (**2**), $C(O)OCH_3$ (**4**) R = H (**3**), $C(O)OCH_3$ (**5**)

Scheme 5 Deprotonation and redox equilibrium of Rh^{III} complexes of TPA ligands.[14]

Upon deprotonation of the N-H proton of the coordinating amide linkage with NEt_3, the redox potential of the Ru^{II}/Ru^{III} couple shifted to +0.17 V, which was lower than that of the Cu^{I}/Cu^{II} couple (+0.40 V). The original potentials can be recovered by adding $HClO_4$. The UV-vis and ESR spectral changes are reversible, indicating the dinuclear complex is stable in the course of protonation and deprotonation. Upon deprotonation, as mentioned above, the redox potentials of Ru and Cu centres show crossover. Therefore, upon deprotonation, intramolecular ET occurs from the Ru(II) centre to the Cu(II) centre, affording a Ru(III)-Cu(I) complex, simultaneously. Reversely, the protonation of the Ru(III)-Cu(I) complex gives the original Ru(II)-Cu(II) complex (Scheme 4). This reversible regulation of the redox states provides new molecular bistability, which has been mentioned as "proton-coupled electron shuttling".[13]

Although the TPA ligand has been used as an auxiliary tetradentate ligand for the preparation of various metal complexes, redox non-innocence of the TPA ligand was not explored. We have prepared a Rh^{III}-TPA complex, $[Rh^{III}Cl_2(TPA)]Cl$ (**1**), and examined the deprotonation of a methylene proton using a strong base such as KOH and 1,8-diazabicyclo[5.4.0]undec-7-ene (DBU) and oxidation of the deprotonated species as shown in Scheme 5.[14] The deprotonation of the TPA ligand coordinated to a Rh^{III} ion occurs selectively at the axial pyridylmethyl moiety due to the higher thermodynamic stability than that of equatorial pyridylmethyl moieties as evidenced by ^1H NMR analysis and DFT calculations. The deprotonation of **1** with a strong base has afforded a deprotonated species, $[Rh^{III}Cl_2(TPA–H^+)]$ (**2**, Scheme 5) and the pK_a value of the methylene proton has been determined to be 27.3 at 294 K on the basis of spectroscopic titration in CH_3CN using DBU (pK_a = 24.3 in CH_3CN) as a base. The cyclic voltammogram of **2** showed one irreversible redox wave at 0.08 V vs. SCE at 233 K in CH_3CN. In order to improve the stability of the deprotonated species on the basis of resonance structures of a metal-bound TPA, we have introduced methoxycarbonyl groups at the 5-position of each pyridine ring of TPA. Thus, another Rh^{III}-TPA complex, $[Rh^{III}Cl_2(MeOC(O)\text{-}TPA)]PF_6$ (**3**, Scheme 5), has been synthesized to examine the deprotonation and redox processes. The deprotonation of **3** has been made using triethylamine (pK_a = 18.8 in CH_3CN), determining the pK_a value of a methylene proton of **3** to be 20.8 at 296 K in CH_3CN. As expected, the deprotonated form of **3**, $[Rh^{III}Cl_2(MeOC(O)\text{-}TPA–H^+)]$ (**4**, Scheme 5), showed a quasi-reversible redox wave at 0.40 V vs. SCE at 233 K in CH_3CN. The one-electron oxidation of **4** by $[Ru(bpy)_3]^{3+}$ in CH_3CN at 233 K afforded a radical species, $[Rh^{III}Cl_2(\{MeOC(O)\text{-}TPA–H^+\}^{\bullet})]$ (**5**, Scheme 5), in which the unpaired electron delocalizes over the axial methine moiety and the 3- and 5-positions of the pyridine ring as demonstrated by DFT calculations. The presence of the unpaired electron has been confirmed by the formation an adduct between **5** and TEMPO as a radical trap as evidenced by ESI-MS spectrometry and ^{1}H NMR spectroscopy. This result indicates that a TPA ligand bound to a strongly Lewis acidic metal centre can be deprotonated to allow us to provide redox-activity of the ligand to create a new category of reactive species.

2. Formation and reactivity of Ru^{IV}-oxo complexes and mechanistic insight into C-H oxidation

Since the first report by Meyer and coworkers in 1978,[7] Ru(II)-aqua complexes can be oxidized by oxidants such as a Ce(IV) salt to generate high-valent Ru-oxo complexes.[8,9] In the course of formation of a Ru^{IV}-oxo complex in a PCET pathway in water, two electrons go to two Ce^{IV} ions and two protons are accepted by water molecules as the solvent, separately. Mechanistic insights into oxidation reactions of water[15] and organic substrates[16] by Ru-oxo complexes have been given to elucidate the reactivity and characteristics of the species. In the case of a Ru^{IV}-oxo complex acting as a reactive species in C-H bond oxidation, a proton is accepted by the oxo ligand and an electron is done by the Ru(IV) centre.

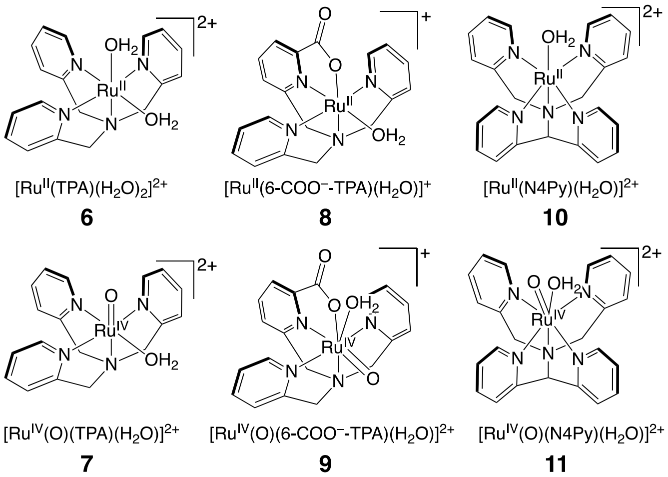

Fig. 1 Schematic descriptions of Ru^{II}-aqua complexes (**6**, **8**, and **10**) and the corresponding Ru^{IV}=O complexes (**7**, **9**, and **11**).

We have prepared a Ru(II)-aqua complex having TPA as a tetradentate ligand to make it possible to perform catalytic oxidation of organic substrates in water, which acts not only as a solvent but also as the sole oxygen source. [Ru^{II}(TPA)(H$_2$O)$_2$]$^{2+}$ (**6**, Fig. 1) can be oxidized by (NH$_4$)$_2$[Ce^{IV}(NO$_3$)$_6$] (CAN) in water to form a Ru^{IV}-oxo complex, [Ru^{IV}(O)(TPA)(H$_2$O)]$^{2+}$ (**7**, Fig. 1), which is in the typical S = 1 spin state, as the reactive species in the oxidation reactions.[17] The first catalytic oxidation of organic substrates has been achieved in water on the basis of PCET oxidation of a Ru^{II}-aqua complex as a catalyst. Catalytic alkene oxidation using this system affords carboxylic acids *via* C=C bond cleavage through the epoxidation followed by diol formation in the acidic aqueous media. In the course of catalytic oxidation of cyclohexene to afford adipic acid, the intermediacy of cyclohexene oxide and cyclohexane 1,2-diol has been

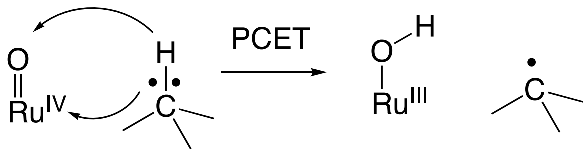

Scheme 6 PCET occurring in the course of hydrogen atom transfer from a C-H bond to a Ru^{IV}=O complex.

confirmed by their oxidation under the same conditions to form adipic acid. The oxygen atoms of adipic acid have been demonstrated to derive from water on the basis of an isotope labelling experiment using H$_2$^{18}O as a solvent.[17]

We have also prepared Ru(II)-aqua complexes having *N*,*N*-bis(2-pyridylmethyl)-*N*-(6-carboxylato-2-pyridylmethyl)-amine (6-COO-TPA) and *N*,*N*-bis(2-pyridyl-methyl)-*N*-bis(2-pyridyl)methylamine (N4Py) as pentadentate ligands, as shown in Fig. 1.[18,19] The two Ru(II)-aqua complexes, [Ru^{II}(6-COO-TPA)(H$_2$O)$_2$]$^+$ (**8**, Fig. 1)[18] and [Ru^{II}(N4Py)(H$_2$O)$_2$]$^{2+}$ (**10**, Fig. 1),[19] are oxidized using CAN in water to generate diamagnetic low-spin (S = 0) Ru^{IV}=O complexes, [Ru^{IV}(O)(6-COO-TPA)(H$_2$O)]$^+$ (**9**, Fig. 1) and [Ru^{IV}(O)(N4Py)(H$_2$O)]$^{2+}$ (**11**, Fig. 1), in seven-coordinate structures with one aqua ligand, which are stabilized by hydrogen bonding with water molecules as supported by DFT calculations.[18,19]

Since we have obtained three different Ru^{IV}=O complexes having similar pyridylamine ligands in the different spin states, we have scrutinized and compared their reactivity in C-H oxidation reactions in light of kinetic analysis. In the PCET reaction, a proton is accepted by the oxo ligand and an electron by the Ru^{IV} centre (Scheme 6). For all three complexes, pseudo-first-order rate constants of alcohol oxidation showed saturation against substrate concentrations, indicating that the Ru^{IV}=O complexes (**7**, **9**, **11**) form adducts with substrates. The use of oxidation-inert hexafluoropropan-2-ol (hfp) as a substrate allowed us to determine the binding constant (5.0 x 10^2 M^{-1}) of hfp with **7** on the basis of titration using ^{19}F NMR spectroscopy in D$_2$O. The downfield shift of the ^{19}F signal derived from the CF$_3$ groups of hfp indicates the formation of hydrogen bonding between a proton of the aqua ligand and the oxygen of hfp even in water. Thus, we concluded that the Ru^{IV}=O complexes with an aqua ligand can form hydrogen

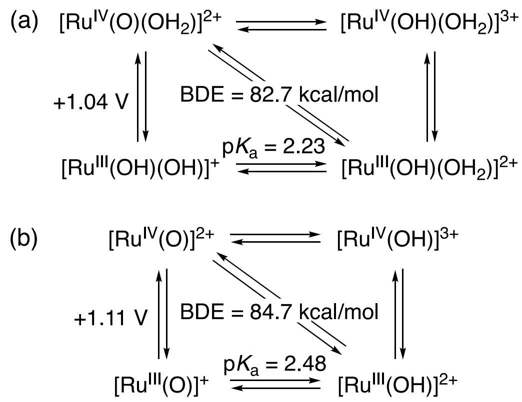

Scheme 7 Thermochemical square schemes for (a) [Ru^{IV}(O)(TPA)(H$_2$O)]$^{2+}$ (**7**) and (b) [Ru^{IV}(O)(N4Py)]$^{2+}$ (**11**).[21] The potentials in water are calibrated relative to NHE.

bonding with alcohols in water prior to the oxidation of entrapped substrates.[20]

On the basis of thermodynamic analysis in light of Pourbaix diagrams of the starting Ru(II)-aqua complexes in water, we could determine the BDE values of Ru^{III}-hydroxo complexes to generate the corresponding Ru^{IV}=O complexes to be 82.7 kcal mol^{-1} for $[Ru^{III}(OH)(TPA)(H_2O)]^{2+}$, 84.7 kcal mol^{-1} for $[Ru^{III}(OH)(N4Py)]^{2+}$ on the basis of eq 1 (Scheme 7). Note that complex **7** is in the S = 1 spin state and complex **11** is in the S = 0 spin state.[21] These data indicate that the hydrogen-abstracting ability of both complexes should be comparable to show not so much difference in the reactivity in C-H oxidation *via* PCET. Thus, we concluded that the spin states of Ru^{IV}=O complexes do not affect the reactivity in HAT from substrates.[22,23]

3. Formation of a Ru^{IV}=O complex through PCET and reaction mechanism of C-H oxidation in CH_3CN

A coordinatively saturated Ru^{II} complex, $[Ru^{II}(TPA)(bpy)]^{2+}$,[24] has been oxidized by CAN in water to generate a Ru^{IV}=O complex, $[Ru^{IV}(O)(\eta^3\text{-}H^+TPA)(bpy)]^{3+}$ (**12**), in which the TPA ligand binds to the Ru^{IV} centre as a tridentate ligand including one uncoordinated and protonated pyridine pendant (Scheme 8).[25] The crystal structure of **12** has been determined by X-ray crystallography. Stoichiometric C-H oxidation in CH_3CN has been examined to elucidate the reaction mechanism on the basis of kinetic analysis and detection of intermediates. In the oxidation of cumene, we can observe a two-step reaction cascade involving a C-H oxidation step and a product substitution step. In the first stage, kinetic isotope effect (KIE) has been observed on the second-order rate constant of cumene oxidation to produce cumyl alcohol. The KIE value was determined to be 12, suggesting contribution of tunneling effect on the hydrogen-atom abstraction. In the course of the reaction, a Ru^{III}-cumyloxo intermediate together with a Ru^{III}-hydroxo complex have been observed by ESI-MS spectrometry. This is the first direct observation of an alcohol-bound complex

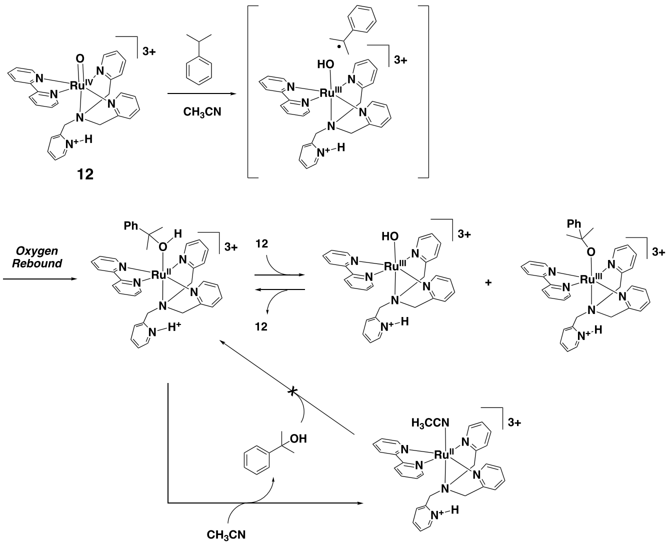

Scheme 8 Proposed mechanism of oxidation of cumene by **12** in CH_3CN.

formed through C-H hydroxylation to provide a direct evidence supporting the “oxygen-rebound” mechanism. The second step obeys first-order kinetics to indicate that the process is a ligand substitution reaction from cumyl alcohol to CH_3CN, forming $[Ru^{II}(\eta^3\text{-}H^+TPA)(bpy)(CH_3CN)]^{3+}$ as the final product. Note that the Ru^{II}-$NCCH_3$ complex does not afford the alcohol or alkoxo complex even in the presence of excess cumyl alcohol in CH_3CN. A proposed reaction mechanism is depicted in Scheme 8.[25]

4. PCET oxidation phenol derivatives by a Ru(III)-hydroxo complex

A Ru^{II}-aqua complex, $[Ru^{II}(Me_2Py5)(H_2O)]^{2+}$ (**13**, Scheme 9), has been synthesized and characterized by various methods.[26] For complex **13**, the pK_a value has been determined to be 11.0 in a Britton-Robinson (BR) buffer at room temperature. The redox potential of the Ru^{II}/Ru^{III} couple of **13** depends on solution pH values with a slope of –57 mV pH^{-1}, indicating that the complex undergoes $1e^-/1H^+$ PCET process. Note that no redox wave assignable to a Ru^{III}-OH/Ru^{IV}=O couple has been observed. The complex **13** can be converted to a Ru^{III}-hydroxo complex, $[Ru^{III}(OH)(Me_2Py5)]^{2+}$ (**14**, Scheme 9), through electrochemical PCET oxidation at 1.3 V (vs. SCE) in a BR buffer at pH 1.3. The complex **14** reacts with phenol derivatives to afford **13** (Scheme 9). The reactions have been kinetically analysed to reveal that the reactions proceed *via* adduct formation between **14** and phenol derivatives, obeying the first-order kinetics, as observed in alcohol oxidation by Ru^{IV}=O complexes mentioned above. The reaction mechanism has been changed from concerted PCET to stepwise ET/PT, depending on the redox potentials of substrates, i.e., the driving force of ET ($-\Delta G_{et}$). When the $-\Delta G_{et}$ is lower than 0.5 eV, the reaction proceeds *via* PCET with showing KIE; however, when it is larger than 0.5 eV, the reactions proceed in an ET/PT mechanism involving non-adiabatic ET, which occurs in a hydrogen-bonded Ru^{III}-OH•••substrate adduct, without showing KIE and the rate constants are on a Marcus parabola with the reorganization energy of 1.31 eV. Thus, the analysis on the basis of the Marcus theory of ET is effective to elucidate the reaction mechanisms. Similar switching of reaction mechanisms has been reported on oxidation reactions of C-H bonds by Cr^V=O and Fe^{IV}=O complexes.[27,28]

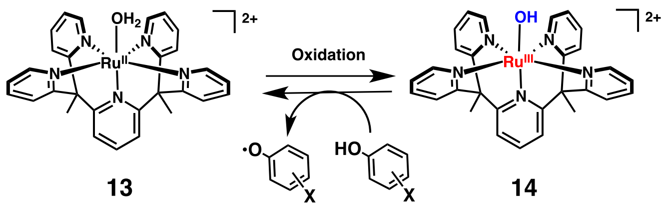

Scheme 9 PCET oxidation of phenol derivatives by the Ru^{III}-OH complex **14** in BR buffer.[26]

5. Formation and reactivity of a Ru^{III}-oxyl complex: Preparation, characterization, and oxidation of organic compounds

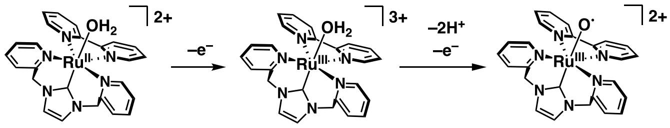

15 16 17

Scheme 10 Formation of a Ru^{III}-oxyl complex through PCET oxidation of a Ru^{II}-aqua complex having an NHC ligand.[31]

When an *N*-heterocyclic carbene (NHC) binds to a metal centre, the NHC ligand has been known to exert strong *trans*-influence due to its strong σ-donating ability to elongate a bond distance between the metal centre and a ligand bound at the *trans* position to the NHC ligand.[29] Thus, an NHC ligand bound at the *trans* position to an oxo ligand can elongate the metal-oxo bond to bring an oxyl character into the oxo ligand. Together with an NHC ligand, we have introduced π-accepting bpy as another auxiliary ligand to enhance the oxyl character.[30]

We synthesized and characterized an orange-coloured Ru^{II}-aqua complex, [Ru^{II}(BPIm)(bpy)(H_2O)](ClO_4)$_2$ (**15**•(ClO_4)$_2$, Scheme 10).[31] The electrochemical analysis on the redox behaviour of the complex allowed us to observe one reversible redox process assigned to the Ru^{II}/Ru^{III} redox couple at +0.86 V vs. NHE and one irreversible process at ~ +1.6 V vs. NHE at pH 2.5 in water. In the Pourbaix diagram of **15**, the redox potential of the first redox process showed no dependence on pH values, assignable to a 1e$^-$ process; however, that of the second step showed a pH dependence with a gradient of –108 mV/pH, indicating that the process should be a 1e$^-$/2H$^+$ process. A blue-coloured one-electron-oxidized species of **15**, [Ru^{III}(BPIm)(bpy)(H_2O)](ClO_4)$_3$ (**16**•(ClO_4)$_2$, Scheme 10), was isolated and characterised by X-ray crystallography and spectroscopic methods. Complex **16** was further oxidized by excess CAN to afford a one-electron-oxidized species. This complex was characterised by various spectroscopic methods and ESI-TOF-MS to be assigned to a Ru^{III}-oxyl complex, [Ru^{III}(O•)(BPIm)(bpy)]$^{2+}$ (**17**, Scheme 10). This complex is formed through 2e$^-$/2H$^+$ PCET oxidation of **15** in strongly acidic water. The resonance Raman spectrum of **17** showed a peak at 731 cm^{-1}, which is much lower than those observed for Ru^{IV}=O complexes (780-833 cm^{-1}). The XANES spectrum of **17** at the Ru-K edge showed a 0.5 eV higher energy at the half-height in comparison with that for **16** and 1.5 eV higher than that of **15**, supporting the oxidation state of the Ru centre in **17** should be closer to Ru^{III} rather than Ru^{IV}. Thus, we have concluded that complex **17** should be described as an unprecedented Ru^{III}-oxyl complex, rather than a Ru^{IV}-oxo complex.

The Ru^{III}-oxyl complex **17** showed unique reactivity in catalytic oxidation of organic substrates in acidic water. Secondary alcohols were oxidized to form the corresponding ketones, styrene-4-sulfonate was oxidized to give a styrene diol derivative probably *via* epoxidation followed by acid-catalyzed hydrolysis of the styrene oxide derivative formed. When benzaldehyde derivatives were used as substrates, the corresponding carboxylic acids were obtained as two-electron oxidized products. A kinetic isotope effect of 8.0 was observed in benzaldehyde oxidation, indicating that hydrogen abstraction from the formyl group is involved in the rate-determining step of the reaction. A Hammett plot for the oxidation of benzaldehyde derivatives gave ρ = –0.07, indicating that the transition state of the oxidation of those substrates does not bear any ionic character to support a strong radical character of **17**.[31]

When benzene derivatives without any electron-withdrawing groups such as sulfonate and trimethylammonium groups are employed as substrates of catalytic oxidation in water, the aromatic rings undergo oxidative cracking to afford formic acid and CO_2, which should be derived from oxidation of formic acid.[32] Surprisingly, aromatic substrates having benzylic moieties were oxidized to afford formic acid and carboxylic acids having the corresponding aromatic substituents; for example, ethylbenzene was oxidized to be formic acid and propionic acid together with CO_2. In addition, no KIE was observed in benzene oxidation, indicating that no hydrogen-atom abstraction occurs from benzene to the reactive species. As a scope of substrates, electron-rich aromatic rings can be oxidatively cracked; however, introduction of electron-withdrawing groups lowered the yield of formic acid. Naphthalene and anthracene were also oxidatively degraded to formic acid.[32]

We have proposed a catalytic mechanism of the benzene cracking as shown in Scheme 11. The electrophilic attack of the Ru^{III}-O• complex to the aromatic ring to form benzene oxide, which is in an equilibrium with oxepin.[33] The equilibrium mixture is further oxidized to give *E*/*Z* isomers of muconic acid,[34] which is further oxidized into formic acid and CO_2. Another pathway is proposed to form *p*-benzoquinone from the equilibrium mixture, as supported by the fact that *p*-benzoquinone can be oxidized to afford formic acid and CO_2 under the reaction conditions.[35]

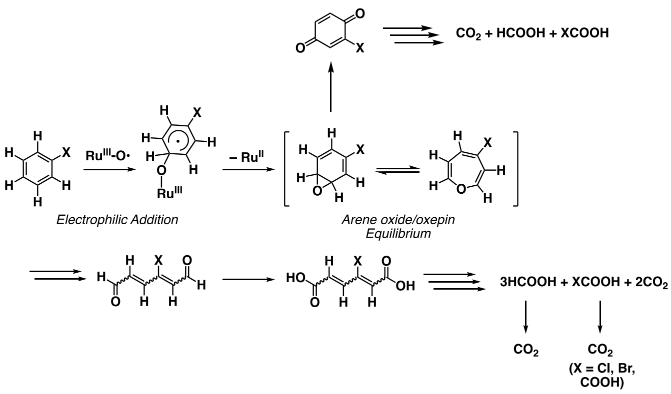

Scheme 11 Proposed mechanisms of oxidative benzene cracking by the Ru^{III}-O• complex **17**.

After oxidative cracking of aromatic compounds in acidic water to generate formic acid, formic acid can be converted to H_2 and CO_2 using a Rh(III) catalyst, [Rh^{III}(Cp*)(bpy)(H_2O)]$^{2+}$,[36] as a catalyst at pH 3.5 in the same solution. Thus, it should be noted that this catalytic system can convert environmentally hazardous aromatic compounds to an energy source, H_2, under mild conditions.

6. PCET from O-H and C-H bonds from substrates to Ru^{III}-pterin complexes

As described in Scheme 1, a PCET reaction occurs from a hydrogen (H^+ and e^-) donor to a proton acceptor and an electron acceptor. In this context, it is not necessarily required to use a high-valent metal-oxo complex as a hydrogen acceptor in PCET. PCET reactions from O-H bonds of phenol derivatives and C-H bonds of hydrocarbons to Ru^{III}-pterin complexes have been investigated on the basis of kinetic analysis.

Two Ru^{II}-pterin complexes, [Ru^{II}(dmp)(TPA)]$^+$ (**18**)[37] and [Ru^{II}(dmdmp)(TPA)]$^+$ (**19**),[38] have been employed for PCET oxidation of phenol derivatives. The difference between **18** and **19** is whether pterin ligands have two methyl groups on the 2-amino group or not; the dmp ligand has the amino group and the dmdmp ligand has the *N*,*N*-dimethylamino group at the 2-position of the pterin framework. Thermochemical square schemes for the two Ru^{II}-pterin complexes were provided to shed lights on the PCET properties in CH_3CN on the basis of

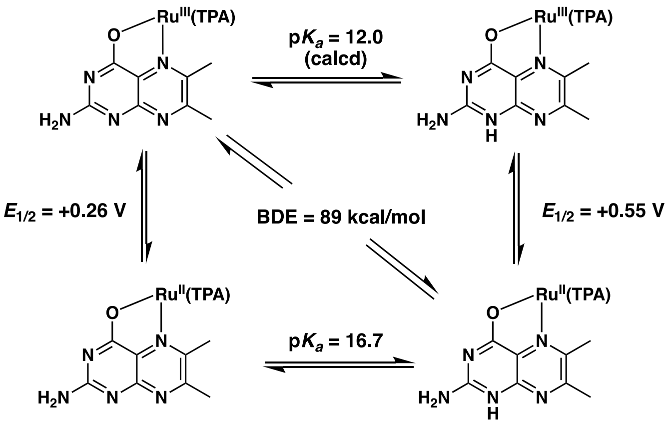

Scheme 12 Thermochemical square scheme for **18** in CH_3CN. $E_{1/2}$ is relative to that of the ferrocene/ferricenium couple.

electrochemical measurements to determine the redox potentials of the Ru centres as electron-accepting sites and spectroscopic titration to determine the pK_a values of the pterin ligands as proton accepting sites. Base on eq 1, BDE of **18** in the PCET process was calculated to be 89 kcal mol^{-1} (Scheme 12)

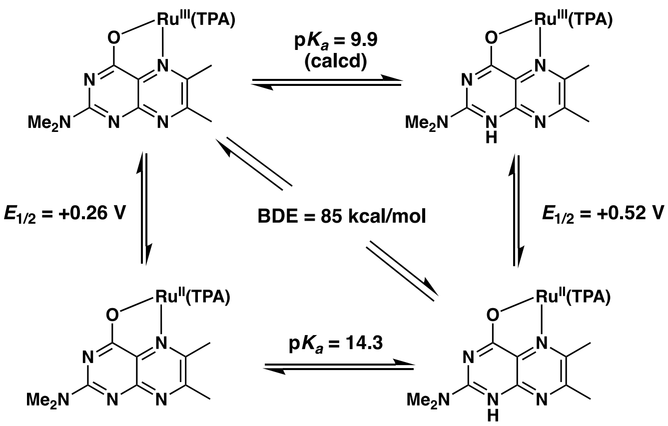

Scheme 13 Thermochemical square scheme for **19** in CH_3CN. $E_{1/2}$ is relative to that of the ferrocene/ferricenium couple.

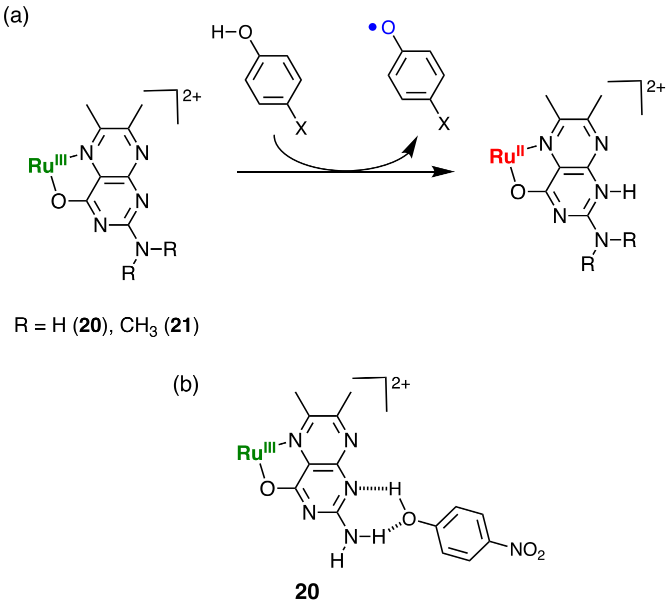

Fig. 2 (a) PCET from phenol derivatives to Ru^{III}-pterin complexes **20** and **21**; (b) A proposed structure of the intermediate in the oxidation of *p*-nitrophenol by **20**.

and that of **19** was done to be 85 kcal mol^{-1} (Scheme 13), which were comparable to those of Ru^{IV}=O complexes mentioned above.[39]

The Ru^{II}-pterin complexes **18** and **19** were oxidized by [Ru^{III}(bpy)$_3$]$^{3+}$ in CH_3CN to generate the corresponding Ru^{III}-pterin complexes, [Ru^{III}(dmp)(TPA)]$^{2+}$ (**20**) and [Ru^{III}(dmdmp)(TPA)]$^{2+}$ (**21**). PCET oxidation reactions of the Ru^{III}-pterin complexes **20** and **21** with a series of phenol derivatives have been examined under pseudo-first-order conditions in CH_3CN at 298 K (Fig. 2(a)).[39] The reactions afforded phenoxyl radicals and the corresponding Ru(II) complexes having protonated pterin ligands that accepted one proton at the 1-*N* position, [Ru^{II}(Hdmp)(TPA)]$^{2+}$ and [Ru^{II}(Hdmdmp)(TPA)]$^{2+}$,[40] as shown in Fig. 2(a). The phenoxyl radical formation was confirmed by ESR spectroscopy to detect 2,4,6-tri-*tert*-butylphenoxyl radical in the reaction of **20** and 2,4,6-tri-*tert*-butylphenol. When highly acidic 4-nitrophenol was examined as a substrate in the reaction with **20**, the pseudo-first-order rate constants showed saturation behaviour against the substrate concentration, suggesting that an adduct between **20** having the amino group at the 2-position of the dmp$^-$ ligand and 4-nitrophenol is formed through two-point hydrogen bonding (Fig 2(b)). The adduct formation was also confirmed by ESI-MS analysis to detect a peak cluster assigned to the adduct. Note that **21** with the *N*,*N*-dimethylamino group at the 2-position of the dmdmp$^-$ ligand did not exhibit such saturation behavior due to the lack of 2-NH_2 group as the hydrogen-bonding site.

The second-order rate constants were determined to shed some lights on the transition states of the reactions in light of the Bell-Evans-Polanyi (BEP) equation (eqns (2) and (3)),[41]

$$E_a = \alpha\Delta H + C \qquad (2)$$

$$\Delta H = \text{BDE (to be formed)} - \text{BDE (to be cleaved)} \qquad (3)$$

where E_a is the activation energy of the reaction, ΔH is the difference between the bond dissociation energy (kcal mol^{-1}) of a bond to be cleaved and that of a bond to be formed, C is a constant in a certain solvent. The coefficient, α ($0 < \alpha < 1$) represents the position of the proton in the transition state of an H-atom transfer (HAT) reaction from an X-H bond to a proton acceptor.[42] The α values of the PCET oxidation reactions of phenols by **20** was determined to be 0.41.[39] This result suggests that the hydrogen atom locates close to the middle of O of a phenol derivative and 1-N of the dmp⁻ ligand in **20**.

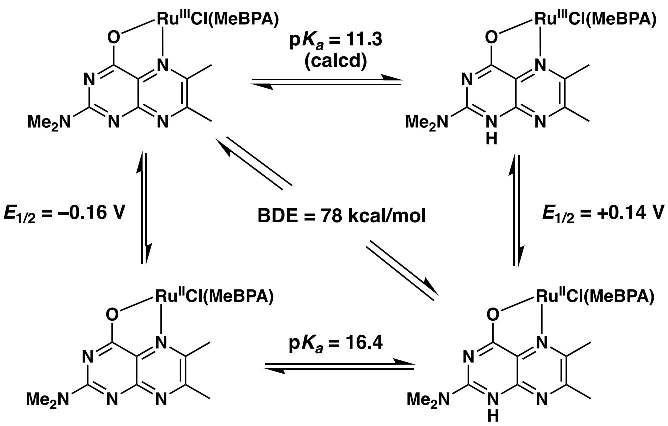

Scheme 14 Thermochemical square scheme for **22** in CH_3CN. $E_{1/2}$ is relative to that of the ferrocene/ferricenium couple.

In place of phenol derivatives, we have examined hydrocarbons as substrates in PCET oxidation by Ru^{III}-pterin complexes in CH_3CN. In order to clarify the impact of pK_a values of pterin ligand as proton acceptor and redox potential of a Ru centre as an electron donor on the transition state of a PCET oxidation reaction, we have prepared a non-charged Ru^{II}-pterin complex having a tridentate ligand, *N*-methyl-*N*,*N*-bis(2-pyridylmethyl)amine (MeBPA), and the chloro ligand, [Ru^{II}(dmdmp)(Cl)(MeBPA)] (**22**).[43] The thermochemical square scheme of **22** has been provided to compare the difference of those parameters (Scheme 14). The redox potentials of the Ru^{II}/Ru^{III} couple are +0.26 V for **19** and –0.16 V for **22**, respectively, indicating the electron acceptability of **19** is higher than that of one-electron-oxidized **22**, [Ru^{III}(dmdmp)(Cl)(MeBPA)]$^+$ (**23**). Based on the square schemes of **19** and **22**, we can estimate the pK_a values of the corresponding Ru^{III} complexes: The values are calculated to be 9.9 for **21** and 11.3 for **23**, respectively, indicating that **23** should show stronger proton acceptability (basicity) than **21**.[43]

The difference of electron acceptability and proton acceptability has been reflected on the α values in eq 4 for the PCET oxidation of C-H bonds of hydrocarbons in CH_3CN at 298 K. The α values of **21** and **23** have been determined to be 0.27 and 0.44, respectively, which are in the range of those for Ru^{IV}=O complexes (0.23-0.44).[8] The difference of the α values indicate that the higher proton acceptability of a ligand causes larger polarization of a C-H bond to facilitate ET from a more negatively polarized carbon atom to a metal centre with lower electron acceptability (Fig. 3).[43] On the contrary, the lower proton acceptability causes less polarization of the C-H bond to require higher electron acceptability to accomplish the PCET oxidation (Fig. 3). DFT calculations on the transition states of PCET oxidation of indene by **21** and **23** have been performed to clarify the situations. As shown in Fig. 4(a), the transition state of PCET from indene to **21** shows a longer N•••H distance (1.46 Å) and shorter C•••H distance (1.29Å); in contrast, as depicted in Fig. 4(b), that of PCET from indene to **23** shows a shorter N•••H distance (1.37 Å) and a longer C•••H distance (1.34 Å). The interatomic distances are consistent with situations reflected on the α values obtained from the BEP plots.

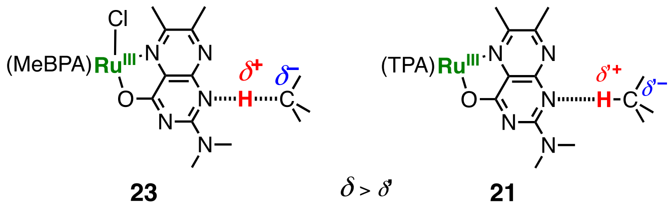

Fig. 3 Proposed arrangements of the transition states in C-H oxidation by **21** and **23**.

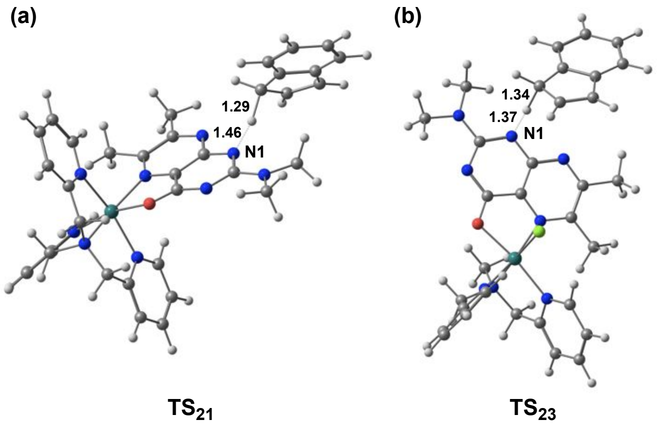

Fig. 4 DFT-optimized transition states of the oxidation of indene by **21** (a) and **23** (b) using the B3LYP method.

The results of PCET oxidation of C-H bonds by Ru^{III}-pterin complexes without oxo ligands clearly demonstrate that the C-H oxidation reactions are controlled by the proton acceptability of a proton acceptor such as an oxo ligand and the electron acceptability of a metal centre.

Conclusions

PCET reactions of transition-metal complexes have been demonstrated to clarify the importance in the development of their valuable functionality. In the formation of high-valent metal-oxo complexes, especially Ru-oxo complexes, PCET is useful for selective formation of targeted species in water which acts not only as a solvent but also as the sole oxygen source in both stoichiometric and catalytic oxidation reactions of organic and inorganic substrates including water. PCET also provides an effective strategy to create a molecular bistability represented by "proton-coupled electron shuttling" in an amide-linked dinuclear Ru^{II}-Cu^{II} complex. Lewis-acid-induced deprotonation of a chelating ligand followed by ET-oxidation affords a ligand radical species with novel electronic structure, which may allow us to achieve further development in catalysis and molecular properties. PCET reactions from organic substrates can be promoted by metal complexes having basic sites as proton acceptors and metal centres as electron acceptors as represented by Ru^{III}-pterin complexes. PCET from O-H and C-H bonds to a complex having an electron-accepting metal centre and a basic and proton-accepting ligand allows us to gain mechanistic insights into the reactions and to understand the controlling factors in the reactivity of metal complexes in PCET.

Conflicts of interest

There are no conflicts to declare.

Acknowledgements

The author appreciates his excellent coworkers including students and prominent experts who appear as co-authors in the references. He would like to share the award for creative work of Japan Society of Coordination Chemistry (JSCC) in 2018 with the coworkers, especially, Dr. Tomoya Ishizuka and Dr. Hiroaki Kotani (University of Tsukuba, Japan) as colleagues for their great efforts to promote research into the present shape. His sincere thanks go to Prof. Shunichi Fukuzumi (Osaka University, Japan and Ewha Womans University, Korea) for his kind support and encouragements, which have been indispensable for the achievements described here. The author appreciates Prof. Yoshihisa Matsuda and Prof. Hiroshi Kitagawa (Kyoto University at present) in Kyushu University for providing opportunities to embark and perform research presented here. The works have been supported by Japan Society of Promotion of Science (JSPS), MEXT, Japan, Japan Science and Technology Agency (JST), The Mitsubishi Foundation, Asahi Glass foundation, Yazaki Memorial Foundation for Science and Technology, The Iwatani Naoji Foundation, and Tsukuba Innovation Arena (TIA).

Notes and references

1 (*a*) S. Hammes-Schiffer, *Acc. Chem. Res.*, 2001, **34**, 273; (*b*) M. H. V. Huynh and T. J. Meyer, *Chem. Rev.*, 2007, **107**, 5004.
2 (*a*) J. W. Darcy, B. Koronkiewicz, G. A. Parade and J. M. Mayer, *Acc. Chem. Res.*, 2018, **51**, 2391; (*b*) J. J. Warren, T. A. Tronic and J. M. Mayer, *Chem. Rev.*, 2010, **110**, 6961.
3 V. D. Parker, K. L. Handoo, F. Roness and M. Tilset, *J. Am. Chem. Soc.*, 1991, **113**, 7439.
4 (*a*) A. Amunts, O. Drory and N. Nelson, *Nature*, 2007, **447**, 58; (*b*) B. Loll, J. Kern, W. Saenger, A. Zouni and J. Biesiadka, *Nature*, 2005, **438**, 1040; (*c*) M. Suga, F. Akita, K. Hirata, G. Ueno, H. Murakami, Y. Nakajima, T. Shimizu, K. Yamashita, M. Yamamoto, H. Ago and J.-R. Shen, *Nature*, 2015**, 517**, 99.
5 (*a*) J. Yano and V. K. Yachandora, *Inorg. Chem.*, 2008, **47**, 1711; (*b*) A. Sartorel, M. Bonchio, S. Campagna and F. Scandola, *Chem. Soc. Rev.*, 2013, **42**, 2262; (*c*) M. Kato, J. Z. Zhang, N. Paul and E. Reisner, *Chem. Soc. Rev.*, 2014, **43**, 6485.
6 (*a*) S. W. Gersten, G. J. Samuels and T. J. Meyer, *J. Am. Chem. Soc.*, 1982, **104**, 4029; (*b*) J. A. Gilbert, D. S. Eggleston, W. R. Murphy, Jr., D. A. Geselowitz, S. W. Gersten, D. J. Hodgson and T. J. Meyer, *J. Am. Chem. Soc.*, 1985, **107**, 3855; (*c*) F. Liu, J. J. Concepcion, J. W. Jurss, T. Cardolaccia, J. L. Templeton and T. J. Meyer, *Inorg. Chem.*, 2008, **47**, 1727.
7 B. A. Moyer and T J. Meyer, *J. Am. Chem. Soc.*, 1978, **100**, 3601.
8 T. Ishizuka, H. Kotani and T. Kojima, *Dalton Trans.*, 2016, **45**, 16727.
9 W. W. Y. Lam, W.-L. Man and T.-C. Lau, *Coord. Chem. Rev.* 2007, **251**, 2238.
10 M. Haga, Md. M. Ali and R. Arakawa, *Angew. Chem. Int. Ed. Engl.*, 1996, **35**, 76.
11 (*a*) T. Kojima, K. Hayashi and Y. Matsuda, *Chem. Lett.*, 2000, 1008; (*b*) T. Kojima, S. Miyazaki, K. Hayashi, Y. Shimazaki, F. Tani, Y. Naruta and Y. Mastuda, *Chem.–Eur. J.*, 2004, **10**, 6402; (*c*) T. Kojima, K. Hayashi, Y. Shiota, Y. Tachi, Y. Naruta, T. Suzuki, K. Uezu and K. Yoshizawa, *Bull. Chem. Soc. Jpn.*, 2005, **78**, 2152; (*d*) T. Kojima, D. Noguchi, T. Nakayama, Y. Inagaki, Y. Shiota, K. Yoshizawa, K. Ohkubo and S. Fukuzumi, *Inorg. Chem.*, 2008, **47**, 886; (*e*) T. Kojima, N. Hirasa, D. Noguchi, T. Ishizuka, S. Miyazaki, Y. Shiota, K. Yoshizawa and S. Fukuzumi, *Inorg. Chem.*, 2010, **49**, 3737; (*f*) S. Miyazaki and T. Kojima, *Current Trends in X-ray Crystallography*, A. Chandrasekaran, ed., Intech, 2011; pp 239-254.
12 T. Kojima, K. Hayashi and Y. Matsuda, *Inorg. Chem*. 2004, **43**, 6793.
13 T. Ishizuka, K. Tobita, Y. Yano, Y. Shiota, K. Yoshizawa, S. Fukuzumi and T. Kojima, *J. Am. Chem. Soc.*, 2011, **133**, 18570.
14 H. Kotani, T. Sugiyama, T. Ishizuka, Y. Shiota, K. Yoshizawa and T. Kojima, *J. Am. Chem. Soc.*, 2015, **137**, 11222.
15 (*a*) T. A. Betley, Q. Wu, T. V. Voorhis and D. G. Nocera, *Inorg. Chem.,* 2008, **47**, 1849; (*b*) X. Sala, I. Romero, M. Rodríguez, L. Escriche and A. Llobet, *Angew. Chem., Int. Ed.* 2009, **48**, 2842; (*c*) J. J. Concepcion, J. W. Jurss, M. K. Brennaman, P. G. Hoertz, A. O. T. Patrocinio, N. Y. M. Iha, J. L. Templeton and T. J. Meyer, *Acc. Chem. Res*., 2009, **42**, 1954; (*d*) X. Sala, S. Maji, R. Bofill, J. García-Antón, L. Escriche and A. Llobet, *Acc. Chem. Res*., 2014, **47***,* 504; (*e*) J. D. Blakemore, R. H. Crabtree and G. W. Brudvig, *Chem. Rev.,* 2015, **115**, 12974; (*f*) L. Duan, L. Wang, F. Li, F. Li and L. Sun, *Acc. Chem. Res*., 2015, **48***,* 2084.
16 (*a*) B. A. Moyer, M. S. Thompson and T. J. Meyer, *J. Am. Chem. Soc.,* 1980, **102**, 2310; (*b*) W. K. Seok, J. C. Dobson and T. J. Meyer, *Inorg. Chem.*, 1988, **27**, 3; (*c*) O. Wiest, K. N. Houk, K. A. Black and B. Thomas, IV, *J. Am. Chem. Soc.,* 1995, **117**, 8594; (*d*) W.-H. Fung, W.-Y. Yu and C.-M. Che, *J. Org. Chem*., 1998**, 63***,* 7715; (*e*) L. K. Stultz, M. Hang, R. A. Binstead, M. Curry and T. J. Meyer, *J. Am. Chem. Soc*., 2000, **122***,* 5984; (*f*) C.-M. Che, K.-W. Cheng, M. C. W. Chan, T.-C. Lau and C.-K. Mak, *J. Org. Chem.*, 2000, **65***,* 7996.
17 Y. Hirai, T. Kojima, Y. Mizutani, Y. Shiota, K. Yoshizawa and S. Fukuzumi, *Angew. Chem., Int. Ed.*, 2008, **47**, 5772.
18 T. Kojima, Y. Hirai, T. Ishizuka, Y. Shiota, K. Yoshizawa, K. Ikemura, T. Ogura and S. Fukuzumi, *Angew. Chem., Int. Ed.*, 2010, **49**, 8449.
19 S. Ohzu, T. Ishizuka, Y. Hirai, H. Jiang, M. Sakaguchi, T. Ogura, S. Fukuzumi and T. Kojima, *Chem. Sci.*, 2012, **3**, 3421.
20 T. Ishizuka, S. Ohzu, H. Kotani, Y. Shiota, K. Yoshizawa and T. Kojima, *Chem. Sci*., 2014, **5***,* 1429.
21 T. Ishizuka, S. Ohzu and T. Kojima, *Synlett*, 2014, **25**, 1667.
22 (*a*) D. Schröder and S. Shaik, *Angew. Chem., Int. Ed.*, 2011, **50**, 3850; (*b*) T. Kojima and S. Fukuzumi, *Angew. Chem., Int. Ed.*, 2011, **50**, 3852.
23 C. T. Saouma and J. M. Mayer, *Chem. Sci.*, 2014, **5**, 21.
24 (*a*) T. Kojima, T. Morimoto, T. Sakamoto, S. Miyazaki and S. Fukuzumi, *Chem.–Eur. J.*, 2008, **14**, 8904; (*b*) T. Kojima, K. Nakayama, M. Sakaguchi, T. Ogura, K. Ohkubo and S. Fukuzumi, *J. Am. Chem. Soc.*, 2011, **133**, 17901.
25 T. Kojima, K. Nakayama, K. Ikemura, T. Ogura and S. Fukuzumi, *J. Am. Chem. Soc.*, 2011, **133**, 11692.

26 S. Ohzu, T. Ishizuka, H. Kotani and T. Kojima, *Chem. Commun.* 2014, **50**, 15018.
27 For a Cr^{V}-oxo complex: H. Kotani, S. Kaida, T. Ishizuka, M. Sakaguchi, T. Ogura, Y. Shiota, K. Yoshizawa and T. Kojima, *Chem. Sci.* 2015, **6**, 945.
28 For Fe^{IV}-oxo complexes: (*a*) Y. Morimoto, J. Park, T. Suenobu, Y.-M. Lee, W. Nam and S. Fukuzumi, *Inorg. Chem*., 2012, **51**, 10025; (*b*) J. Park, Y. Morimoto, Y.-M. Lee, W. Nam and S. Fukuzumi, *Inorg. Chem*., 2014, **53**, 3618.
29 J. M. Smith and J. R. Long, *Inorg. Chem*. 2010, **49**, 11223.
30 Y. Shimoyama and T. Kojima, *Inorg. Chem.*, 2019, **58**, 9517.
31 Y. Shimoyama, T. Ishizuka, H. Kotani, Y. Shiota, K. Yoshizawa, K. Mieda, T. Ogura, T. Okajima, S. Nozawa and T. Kojima, *Angew. Chem., Int. Ed.*, 2016, **55**, 14041.
32 Y. Shimoyama, T. Ishizuka, H. Kotani and T. Kojima, *ACS Catal.*, 2019, **9**, 671.
33 E. Vogel and H. Günther, *Angew. Chem., Int. Ed. Engl.*, 1967, **6**, 385.
34 B. T. Golding, M. L. Barnes, C. Bleasdale, Y.-F. Tsai, C.-C. Liu, C.-Y. Mou and S. S.-F. Yu, *Chem.-Biol. Interact.*, 2010, **184**, 196.
35 R. Ramu, W. H. Wanna, D. Janmanchi, Y.-F. Tsai, C.-C. Liu, C.-Y. Mou and S. S.-F. Yu, *Mol. Catal.*, 2017, **441**, 114.
36 S. Fukuzumi, T. Kobayashi and T. Suenobu, *ChemSusChem*, 2008, **1**, 827.
37 S. Miyazaki, T. Kojima, T. Sakamoto, T. Matsumoto, K. Ohkubo, S. Fukuzumi, *Inorg. Chem.*, 2008, **47**, 333.
38 T. Kojima, T. Sakamoto, Y. Matsuda, K. Ohkubo, S. Fukuzumi, *Angew. Chem., Int. Ed.*, 2003, **42**, 4951.
39 S. Miyazaki, T. Kojima, J. M. Mayer, S. Fukuzumi, *J. Am. Chem. Soc.*, 2009, **131**, 11615.
40 S. Miyazaki, K. Ohkubo, T. Kojima, S. Fukuzumi, *Angew. Chem., Int. Ed.*, 2008, **47**, 9669.
41 M. G. Evans and M. Polanyi, *Trans. Faraday Soc.*, 1938, **34**, 11.
42 (*a*) J. E. Leffler, *Science*, 1953, **117**, 340; (*b*) J. R. Murdoch, *J. Am. Chem. Soc.*, 1972, **94**, 4410.
43 H. Mitome, T. Ishizuka, H. Kotani, Y. Shiota, K. Yoshizawa and T. Kojima, *J. Am. Chem. Soc.*, 2016, **138**, 9508.

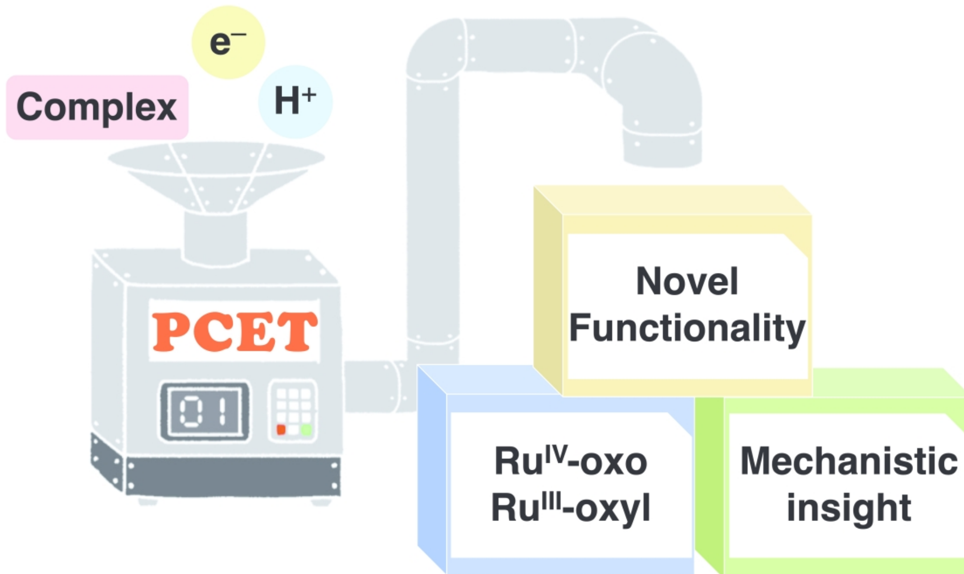

350x207mm (300 x 300 DPI)